Benjamin Schuler, Everett A. Lipman, Peter J. Steinbach, Michael Kumke, William A. Eaton

Polyproline and the „spectroscopic ruler“ revisited with single-molecule fluorescence

first published in:
Proceedings of the National Academy of Scienes of the United States of America. - ISSN 1091-6490. - 102 (2005), 8, p. 2754 - 2759
doi: 10.1073/pnas.0408164102

Polyproline and the "spectroscopic ruler" revisited with single molecule fluorescence

Submitted to *PNAS*, Track II, November 2, 2004
(Biological Sciences/Biophysics)

Benjamin Schuler[*†,‡], Everett A. Lipman[*,§], Peter J. Steinbach[¶], Michael Kumke,[‖] and William A. Eaton[*]

*Laboratory of Chemical Physics, National Institute of Digestive and Diabetes and Kidney Diseases, and [¶]Center for Molecular Modeling, Center for Information Technology, National Institutes of Health, Bethesda, MD, 20892-0520; [†]Physikalische Biochemie and [‖]Institut für Physikalische Chemie, Universität Potsdam, D-14476 Golm, Germany

[‡]Present address: Biochemisches Institut, Universität Zürich, CH-8057 Zürich, Switzerland

[§]Present address: Department of Physics, University of California, Santa Barbara, CA 93106

Corresponding author: William A. Eaton, Building 5, Room 104, NIH, Bethesda, MD 20892-0520; tel: (301) 496-6030, fax: (301) 496-0825, email: eaton@helix.nih.gov

Manuscript length: 18 text pages, 4 figures, 168 word abstract, 45,011 total character count.

Abstract

To determine whether Förster resonance-energy transfer (FRET) measurements can provide quantitative distance information in single molecule fluorescence experiments on polypeptides, we have measured FRET efficiency distributions for donor and acceptor dyes attached to the ends of freely diffusing polyproline molecules of various lengths. The observed mean FRET efficiencies agree with those determined from ensemble lifetime measurements, but differ considerably from the values expected from Förster theory with polyproline treated as a rigid rod. At donor-acceptor distances much less than the Förster radius R_0, the observed efficiencies are lower than predicted, while at distances comparable to and greater than R_0, they are much higher. Two possible contributions to the former are incomplete orientational averaging during the donor lifetime and, because of the large size of the dyes, breakdown of the point-dipole approximation assumed in Förster theory. End-to-end distance distributions and correlation times obtained from Langevin molecular dynamics simulations suggest that the differences for the longer polyproline peptides can be explained by chain bending, which considerably shortens the donor-acceptor distances.

Introduction

Almost 40 years ago, Förster resonance energy transfer (FRET) was introduced in classic experiments by Stryer and Haugland as a "spectroscopic ruler" to measure distances in macromolecules (1). Since then it has been used to address a wide range of biological questions (2-5). More recently, renewed interest has come from the realization that FRET can be used for obtaining distance information in experiments on single biomolecules (6, 7), with a considerable body of work on proteins and polypeptides (8-24). However, it is well known from ensemble experiments that determination of distances from FRET can be complicated by dynamical effects, as well as photophysical, photochemical, and instrumental factors (25). Are there additional complications in single molecule experiments on polypeptides and proteins? To investigate this question, we have studied FRET between dyes attached to the N- and C-termini of polyproline of various lengths. Polyproline, assumed to be a rigid rod, was used as a spacer by Stryer and Haugland to show that the rate of FRET depends on the inverse sixth power of the donor-acceptor distance, as predicted by Förster theory (26).

FRET of individual, dye-labeled poylproline molecules freely diffusing in solution was investigated using a confocal fluorescence microscope setup (13). If a molecule diffuses into the volume illuminated by the focused laser beam, the donor dye is excited. Depending on the distance to the acceptor, a certain rate of energy transfer results, which determines the FRET efficiency, calculated from the fraction of photons emitted by the acceptor. To test the accuracy of the single molecule results, we also determined FRET efficiencies from ensemble measurements of donor lifetimes in the presence and absence of acceptor using time-correlated single photon counting (TCSPC).

Because the FRET efficiencies for the longer peptides were found to be considerably higher than those expected for polyproline treated as a rigid rod, we carried out Langevin molecular dynamics simulations of polyproline of varying lengths. The calculations show that the longer peptides are quite flexible, with end-to-end distance distributions and correlation times that can account for the observed FRET efficiencies.

Material and Methods

Peptide preparation. Polyproline peptides of defined length, containing 6, 9, 11, 12, 13, 15, 20, 23, 27, 33 and 40 Pro residues, respectively, were synthesized using standard FastMoc chemistry with a Model 433A peptide synthesizer (Applied Biosystems, Foster City, CA) on Fmoc-Cys(Xan)-Wang resin (Peptides International, Louisville, KY). We included an amino terminal glycine and the carboxy terminal cysteine residue, which react via their amino and sulfhydryl groups, respectively, with succinimide esters and maleimide derivatives of the dyes. After cleavage, the raw material was purified by reversed phase HPLC on a Vydac (Columbia, MD) C4 column (214TP1022) at a flow rate of 5 ml/min over 45 min using a linear gradient from 0.1% trifluoro acetic acid (TFA) in 10% acetonitrile/90% water to 0.1% TFA in 90% acetonitrile/10% water. Fractions containing the pure peptide as confirmed by electrospray ionization mass spectroscopy were lyophilized, dissolved in buffer and labeled with Alexa Fluor 488 maleimide (27) at 4 °C for 12 h under the conditions recommended by Molecular Probes (Eugene, OR). Singly labeled peptide was purified on a Superdex Peptide HR 10/30 size-exclusion chromatography column (Amersham Biosciences, Piscataway, NJ) in 100 mM sodium carbonate buffer, 0.001% Tween 20, pH 8.3, concentrated to about 1 mM and labeled by addition of a 20% molar surplus of Alexa Fluor 594 succinimidyl ester and

incubation at 20 °C for 1 h. Doubly labeled peptide was purified by a second size-exclusion chromatography run, frozen in liquid nitrogen and stored at -85 °C.

Confocal fluorescence microscope. Observations of single-molecule fluorescence were made using a custom confocal microscope as described previously (13). A 1.4 NA, 100x microscope objective (Nikon CFN Plan Apo 85025) was coupled with immersion oil to one face of a sample cuvette, consisting of two fused silica coverslips (Esco R425025) separated by 180 μm glass spacers. Light from the 488 nm line of an argon ion laser (Lexel 95-5) was made circularly polarized using a single-mode fiber polarization controller (Thorlabs FPC560) and filtered (CVI F03-488.0-4-1.00) to remove unwanted luminescence from the laser tube discharge and optical fibre. The sample was illuminated via a dichroic mirror (Omega Optical 505DRLP) and the objective in a standard epifluorescence arrangement. Sample fluorescence, transmitted by the dichroic mirror, passed through a 100 μm diameter pinhole in the image plane of the objective. After further filtering (Omega 495AELP) to remove scattered laser light, the fluorescence was separated into donor and acceptor components using a second dichroic mirror (Omega 560DCLP) and two final filters (Omega 525AF45 for the donor and Omega 600ALP for the acceptor). Each component was focused onto a photon counting avalanche photodiode (PerkinElmer Optoelectronics SPCM-AQR-15). Output pulses, corresponding to individual detections, from the photodiode modules were collected in 1 ms intervals by a pair of multichannel scalers (EG&G PAR 914P).

Single molecule measurements. For single molecule experiments, samples of labeled peptides were diluted to a concentration of 35 pM in 50 mM sodium phosphate adjusted to pH 7, containing 0.001% Tween 20 to prevent surface adhesion of the polypeptides. Ensemble experiments were performed in a Spex Fluorolog 2 under identical buffer conditions at peptide concentrations of 10 nM. R_0 = 5.4 nm for this dye pair in water was calculated from the measured overlap integral of the normalized donor emission and acceptor absorption spectra (with a peak extinction coefficient supplied by Molecular Probes of 7.8 $10^5\,M^{-1}cm^{-1}$), a donor fluorescence quantum yield of 0.5 and a refractive index of 1.33. Even for higher values of the donor fluorescence quantum yield, R_0 would not increase beyond 6 nm.

Time correlated single photon counting. Fluorescence lifetime and anisotropy decay measurements were performed with a FL920 fluorimeter (Edinburgh Instruments, Livingston, UK). A frequency doubled titanium sapphire laser system (Tsunami 3960; Spectra Physics,

Mountain View, USA) set to λ_{ex} = 435 nm was used as the excitation light source. The excitation pulse width was determined to 100 fs using an autocorrelator (Pulse Check; APE, Berlin, Germany), and the laser repetition rate of 80 MHz was reduced to 1 MHz with a pulse picker (Pulse Select; APE, Berlin, Germany). Fluorescence decays were measured with a multichannel plate (ELDY EM1-132/300 MCP-PMT, Europhoton, Berlin, Germany). The complete detection system has an instrumental response time of ~100 ps. For anisotropy decay experiments, emission with vertical (vv) and horizontal (vh) polarization with respect to the vertically polarized excitation laser beam was measured using a polarization filter. For data analysis, the commercial software package provided with the FL920 fluorescence spectrometer was used. The experimental fluorescence decay data were iteratively deconvolved from the instrument response function based on a Marquardt algorithm and fit to a single exponential. No attempt was made to extract end-to-end distributions or diffusion coefficients from a more detailed analysis of the decay curves (4). Analysis of anisotropy decay measurements was performed by calculating the anisotropy from the vv and vh intensity decay curves after tail matching.

Molecular dynamics simulations. Langevin molecular dynamics simulations were performed for each of seven polypeptides of the form Gly-Pro$_n$-Cys, where n = 10, 15, 20, 25, 30, 35, or 40. The starting conformation of each peptide was obtained by appending extended Gly and Cys residues to poly-proline modeled in a type II helix using the angular parameters derived from the crystal structure (28). All simulations were performed using the EEF1 implicit-solvent energy function (29) implemented in the program CHARMM (30). The EEF1 effective energy function involves a polar-hydrogen description of the peptide solute and a solvation free energy model. EEF1 has been successfully used to discriminate native protein folds from misfolded decoy structures (31) and in structure-prediction simulations of three peptides of known structure (32). Following minimization of the EEF1 energy to a root mean-square gradient less than 0.005 kcal/mol/A, the dynamics of each peptide were simulated at 298 K with a collision frequency of 50/ps applied to all heavy (non-hydrogen) atoms, the SHAKE algorithm (33) applied to the four bonds involving hydrogen atoms (in the terminal residues), and a 2-fs time step. Atomic coordinates were saved every 2 ps. Between 1.5 and 4 microseconds of dynamics were analyzed for each peptide.

Results

Energy transfer from the green-fluorescing donor dye (Alexa Fluor 488) at the carboxy-terminus to the red-fluorescing acceptor dye (Alexa Fluor 594) at the amino-terminus was measured by determining the fraction of acceptor photons in bursts from individual molecules containing 100 detected photons or more, and constructing histograms of FRET efficiencies ($E \equiv n_A/(n_A + n_D)$, where E is the transfer efficiency, n_D and n_A are the numbers of counts in the donor and acceptor channels, respectively) calculated from the individual bursts. Figure 1 shows the results for a subset of the polyproline peptides investigated. As expected, the mean transfer efficiencies decrease with increasing peptide length. The histograms show a maximum at transfer efficiencies ranging from about 0.95 for the six-residue peptide to 0.2 for the 40-residue peptide (Figs. 1 and 2). The additional peak at a transfer efficiency close to zero is due to molecules lacking an acceptor chromophore, and was not included in the calculation of mean transfer efficiencies. The peak near zero efficiency increases with increasing laser intensity and with the size of the molecule, while in previous experiments (16) it was found to be virtually absent when the solution was flowed. These observations suggest that the acceptor chromophore undergoes a photochemical change before entering the confocal volume.

Surprisingly, even for peptides with more than 30 residues, a large amount of transfer was observed. Assuming the same rigid geometry of polyproline as observed in the crystal structure (28), these peptide lengths would correspond to end-to-end distances of more than 10 nm, and the resulting calculated transfer efficiencies for the dye pair used would be less than 3 %, which would be inseparable from the peak near zero efficiency. A comparison with the Förster curve assuming a fixed distance r between the dyes,

$$E = \left(1+\left(r/R_0\right)^6\right)^{-1} \qquad (1)$$

illustrates the dramatically increased FRET efficiencies for long polyproline peptides (Fig. 2A), where $R_0 = 5.4$ nm is the Förster radius (the distance of 50% excitation energy transfer) for this dye pair calculated assuming complete orientational averaging of the dye transition dipoles (25). This raises two questions. Are the single molecule FRET efficiencies accurate? Is it valid to assume that polyproline is a rigid rod for the longer peptides?

A potential complication in single molecule experiments arises from differences in the photon collection efficiencies of the two detection channels corresponding to donor and acceptor emission. This effect can be corrected for by introducing into the equation used to calculate the transfer efficiency from the experimental data a factor γ that accounts for differences in the detection efficiencies of the emission channels and fluorescence quantum yields of the dyes (34), i.e. $E \equiv n_A/(n_A + \gamma n_D)$; γ must be determined for the particular experimental setup and pair of chromophores. For the instrument and dyes used here, we had previously compared single molecule and ensemble FRET efficiencies measured with a calibrated spectrofluorimeter to show that γ is approximately 1 (13). To further test this approximation, we performed time-correlated single photon counting measurements on bulk samples of labeled polyproline to determine FRET efficiencies from the fluorescence lifetime of the donor chromophore as a function of peptide length. The FRET efficiency is given by $(1- \tau_{DA}/\tau_D)$, where τ_{DA} and τ_D are the donor lifetimes in the presence and absence of acceptor, respectively. As shown in Figure 2, the efficiencies from the lifetime measurements are in good agreement with those from the single molecule intensity measurements, eliminating the possibility of the high efficiencies arising from $\gamma < 1$.

For the shortest peptides, a significantly lower transfer efficiency than expected is observed experimentally. Polarization measurements point to a possible reason for decreased energy transfer. For the shortest polyproline peptides, an increase in the steady state residual anisotropy is observed for the donor, from about 0.05 for the longest peptides, to 0.11 for the hexaproline peptide: the decrease in the lifetime of the excited state of the donor due to the very rapid energy transfer to the acceptor no longer permits complete orientational averaging of the chromophores. Consequently, the value of 2/3 for the orientation factor κ^2 derived assuming rapid orientational averaging, and most commonly used for the analysis of FRET experiments in solution, is not applicable. As a limiting case, we calculated the distance dependence of the mean transfer efficiency $\langle E \rangle$ for dyes with a fixed separation and random, but static, relative transition dipole orientations, from the isotropic probability density $p(\kappa^2)$ using**

$$\langle E \rangle(r) = \int_0^4 E(r,\kappa^2)\, p(\kappa^2)\, d\kappa^2 \qquad \text{with} \qquad E(r,\kappa^2) = \left(1 + \frac{2}{3\kappa^2} \left(r/R_0 \right)^6 \right)^{-1}. \qquad (2)$$

The result shows a decreased FRET efficiency for small distances (Fig. 2A), providing an upper bound on the influence of a lack of orientational averaging.

The larger discrepancy with equation (1) is observed for the longer polyprolines (Fig. 2A). To investigate the influence of the polypeptide bending, which would bring the dyes closer together, providing an explanation for the higher FRET efficiency of the long polyprolines, we performed Langevin molecular dynamics simulations. Trajectories of several microseconds were computed for a range of polypeptide lengths. The simulations included the glycine and cysteine residues at the termni, but not the dyes. The starting structure was a polyproline type II helix modeled according to the crystal structure (28). The simulations reveal considerable bending of the peptides, especially for the higher oligomers. Because of the strong distance dependence of Förster transfer, this will make a significant contribution to an increase in transfer efficiency between the dyes on the termini, particularly for the longer peptides. The ends of the polypeptide containing 40 proline residues, which has a contour length of ~12 nm, can get to within ~6 nm in the simulation (Fig. 3), corresponding to an increase in the (instantaneous) transfer rate by a factor of $\sim 2^6$.

The end-to-end distance distributions obtained from the simulations are very similar to those of a worm-like chain. To obtain an estimate of the persistence length, the distributions were fit with the equation of Bhattacharjee *et al.*, which provides a good approximation for the end-to-end distance distribution $P(r)$ of a semiflexible chain (35):

$$P(r) = \frac{4\pi N r^2}{l_c^2\left(1 - r^2/l_c^2\right)^{9/2}} \exp\left(-\frac{9 l_c}{8 l_p\left(1 - r^2/l_c^2\right)}\right) \tag{3}$$

where r is the end-to-end distance, l_c and l_p are the contour length and the persistence length of the chain, respectively, and N is a normalization constant. The fits of the wormlike chain model to the data give a persistence length of 7 ± 1 nm. (Fig. 3). The apparently smaller persistence lengths for the shortest peptides may be due to the larger deviations of the fits at the short distance ends of the distributions.

A quantitative determination of the influence of chain bending on the mean FRET efficiency also requires consideration of the time scale of the end-to-end distance fluctuations and the donor fluorescence lifetime (36, 37). Figure 4 summarizes the relevant times. The typical duration of a photon burst in our experiments is ~1 ms, much longer than the donor fluorescence lifetime or the end-to-end distance correlation time, resulting in complete

conformational averaging during the observation time for an individual molecule. The fluorescence lifetimes of the donor, as determined by TCSPC measurements, range from about 0.4 to 3.6 ns for the different labeled peptides. The reorientational correlation time of the donor chromophore is about 0.3 ns as determined from the anisotropy decay of donor-labeled peptide in the absence of transfer. Chain dynamics were quantified from the molecular dynamics simulations by calculating the autocorrelation functions of the end-to-end distance fluctuations and fitting them to single exponential decays. The resulting relaxation times are between ~0.2 ns for the proline decamer to about 10 ns for the longest peptides (Fig. 4). Chain dynamics and fluorescence decay are in a very similar range for all peptides, and for the shortest chains, the donor fluorescence lifetime approaches the re-orientational correlation time, as expected from the corresponding increase in residual anisotropy mentioned above. Therefore, we should consider all three physically plausible limits for the possible averaging regimes:

1. If the rotational correlation time τ_c of the chromophores is small relative to the fluorescence lifetime τ_f of the donor, and the dynamics of the polyproline chain (with relaxation time τ_p) are slow relative to τ_f,

$$\langle E \rangle = \int_a^{l_c} E(r)P(r)\,dr \text{ with } E(r) = \left(1 + \left(r/R_0\right)^6\right)^{-1} \tag{4}.$$

where $P(r)$ is the normalized inter-dye distance distribution and a is the distance of closest approach of the dyes.

2. If $\tau_c << \tau_f$ and $\tau_p << \tau_f$,

$$\langle E \rangle = \frac{\int_a^{l_c} \left(R_0/r\right)^6 P(r)\,dr}{1 + \int_a^{l_c} \left(R_0/r\right)^6 P(r)\,dr} \tag{5}.$$

3. If $\tau_c >> \tau_f$ and $\tau_p >> \tau_f$,

$$\langle E \rangle = \int_0^4 \int_a^{d_c} E(r,\kappa^2)\, P(r)\, p(\kappa^2)\, dr\, d\kappa^2 \text{ with } E(r,\kappa^2) = \left(1 + \frac{2}{3\kappa^2}\left(r/R_0\right)^6\right)^{-1} \qquad (6).$$

In all cases we used the normalized end-to-end distance distributions from the molecular dynamics simulations, $P(r)$ (Fig. 3) and the theoretical isotropic probability density $p(\kappa^2)$ to calculate the mean transfer efficiencies for the polyproline peptides studied by simulation.** The results are plotted in Figure 2B and illustrate that the flexibility of the chains results in markedly increased transfer efficiencies compared to those calculated for rod-like molecules (Fig. 2A). Moreover, they demonstrate the strong influence of the different dynamic regimes. Considering that $\tau_c << \tau_f$ and $\tau_p \approx \tau_f$ for the longer oligomers, we expect the corresponding experimental results to be in the range of the values calculated with Eq. 4 and 5. The static limit (Eq. 6) will only be relevant for the shortest peptides. All in all, chain flexibility and dynamics account well for the experimentally observed mean transfer efficiencies.

We should mention that in the simulations of the 30- and 35-mer, sudden transitions to long-lived kinked structures were observed but were excluded from our analysis (Figures 3,4). We suspect that these structures are an artifact that reflects our use of an implicit solvent model and will require further investigation with explicit solvent. Such structures would increase the calculated mean FRET efficiency, bringing the calculated values in even closer agreement with the observed.

Discussion

To determine whether Förster resonance energy transfer (FRET) measurements can provide quantitative distance information in single molecule fluorescence experiments, we have measured the FRET efficiency for donor and acceptor dyes attached to the ends of freely-diffusing polyproline molecules of various lengths. Polyproline, the stiffest homo-oligopeptide (38), forms a type II trans helix with a pitch of 0.31 nm per residue in aqueous solution (28), and its conformation does not change upon addition of denaturants (13). However, our experimentally observed inter-dye distance dependence of the mean FRET efficiency differs greatly from the predictions of the simplest Förster formula, Eq. 1, assuming

a perfectly rigid rod for the polyproline spacer and fast, isotropic rotational averaging of the chromophores (Figure 2A). For peptides with a length much shorter than the size of the Förster radius, too low a transfer efficiency is observed; for longer peptides, the transfer efficiency is substantially higher than expected for a rod-like behavior of polyproline. The differences are not a result of inaccuracies in the single molecule measurements, since the mean efficiencies have been confirmed with ensemble lifetime measurements

Two factors may contribute to the deviations for the smallest oligomers. One is the lack of orientational averaging during the donor lifetime, as indicated by the decay of the anisotropy (inset to Figure 4), so that the average angular factor $\kappa^2 < 2/3$. Our calculations (equations 2 and 6) provide an upper bound on this effect, and the experimental data are well within the expected range (Fig. 2). The second is the breakdown of the point dipole approximation of Förster theory, which requires that the size of the donor and acceptor be small compared to their intermolecular separation. In the present case, the lengths of both donor (0.7 nm) and acceptor (1.2 nm) dyes are not small compared to the length of the 10-residue polyproline spacer of ~3 nm. The point dipole approximation leads to the important property of the theory that all of the parameters can be directly calculated from experimental measurables. If this is not true, the rate must be calculated from a detailed quantum mechanical treatment of the Coulomb interaction between the charge distributions (39-41), which is not nearly as reliable and could lead to either a faster or slower rate of excitation energy transfer, i.e. either a higher or lower FRET efficiency than predicted using the point dipole approximation.

For the long peptides, Langevin molecular dynamics simulations show that the difference can be explained by the flexibility of polyproline. The decay of the autocorrelation function indicates that the end-to-end distance distribution is completely sampled within the 1 ms collection time of photons from individual molecules. By considering the averaging regimes relevant for the reorientation of the dyes and the fluctuations of the end-to-end distances of the chains, the main components contributing to the enhancement of the mean FRET efficiencies are accounted for (Figure 2B). A more complete analysis would include the donor and acceptor dyes and their linkers in simulations with explicit solvent, and a direct calculation of the FRET efficiency, as was done, for example, in the case of Förster transfer of excitation energy from tryptophan to heme calculated using an all-atom molecular dynamics trajectory of myoglobin (42).

Polyproline peptides were first used in the context of FRET in the work of Stryer and Haugland (1), who experimentally observed the distance dependence of the transfer efficiency

predicted by Förster (26), assuming polyproline to be a rigid rod. For the longer polyprolines used in the present work, however, the end-to-end distance distributions obtained from Langevin molecular dynamics simulations are not those of a rigid rod, but are much more like the distributions of a worm-like chain (43). To extract an apparent persistence length, the end-to-end distributions were fit with the model function of Bhattacherjee *et al*., equation 3 (35) (Figure 3). The persistence length obtained from the fits is 7 ± 1 nm, significantly less than the textbook value of 22 nm (38, 43), indicating greater flexibility than previously thought. However, in the range of the small peptide lengths used by Stryer and Haugland (up to the dodecamer), polyproline can be well approximated by a rigid rod. [††]

Interestingly, since the experiments of Haugland and Stryer, there have been very few studies of the distance dependence of the FRET efficiency and no rigorous determination of the accuracy of Förster theory at distances for which the point dipole approximation should apply. In the only previous single molecule study of the distance dependence, Deniz *et al*. (44) used B-form, double-stranded DNA as a spacer between large donor and acceptor dyes. Using the reported R_0 = 5.3 nm and an assumed correction factor γ = 1, the measured FRET efficiency was also found to be much higher than the predictions of equation 1, even though flexibility can play no role, because the persistence length of DNA is about 10-fold larger than the R_0 of the donor/acceptor dye pair. However, a very recent reinvestigation has found excellent agreement between measured and predicted FRET efficiencies, by including dye flexibility, by using alternating laser excitation of the donor and acceptor to eliminate the zero-efficiency peak (45), by determining a more accurate value for the correction factor γ, and by re-determining R_0 from spectroscopic data to be 6.9 nm (N. K. Lee, A. N. Kapanidis, Y. Wang, X. Michalet, J. Mukhopadhyay, R. H. Ebright, and S. Weiss, personal communication of submitted manuscript).

Polyproline has been used as a spectroscopic reference for single molecule fluorescence experiments (13), and due to the large number of potential photochemical complications in single molecule studies on biomolecular dynamics, we expect labeled polyproline peptides to become an important standard for calibrating measurements and for testing and refining new experimental methods. For single molecule FRET experiments on proteins, it is desirable to use a polypeptide-based reference molecule, because the type of attachment chemistry and the characteristics of the immediate molecular environment can influence the photophysical properties of fluorophores (46, 47). Single molecule measurements have the advantage that they provide distributions, and that they can be used to

separate subpopulations and to investigate their dynamics individually. Even though the chromophores necessary for these studies are relatively large, our results show that, in principle, there are no additional complications in single molecule experiments other than those arising from photodestruction due to multiple excitations at the high laser intensities used. As in ensemble FRET experiments, consideration of the dynamics is critical for extracting structural information.

Footnotes

**For the case in which all orientations of the donor and acceptor transition dipoles are equally probable (25, 48)

$$p(\kappa^2) = \begin{cases} \dfrac{1}{2\sqrt{3\kappa^2}} \ln(2+\sqrt{3}) & 0 \le \kappa^2 \le 1 \\ \dfrac{1}{2\sqrt{3\kappa^2}} \ln\left(\dfrac{2+\sqrt{3}}{\sqrt{\kappa^2} + \sqrt{\kappa^2 - 1}} \right) & 1 \le \kappa^2 \le 4 \end{cases}$$

with $\kappa^2 = \left(\cos\theta_T - 3\cos\theta_D \cos\theta_A \right)^2$, where θ_T is the angle between the donor and acceptor transition dipoles, θ_D and θ_A are the angles between the transition moments and the line connecting the centers of the donor and acceptor, respectively.

††Stryer and Haugland also fit their data using an R_0 of 3.4 nm instead of the value of 2.7 nm obtained from the measured spectroscopic parameters. The difference between their experimental data and the curve predicted from equation 1 with R_0 = 2.7 nm can largely be accounted for by assuming the dye linkers to be flexible instead of stiff extensions of the chain.

Acknowledgements: We thank Attila Szabo and Irina Gopich for many helpful discussions. We also thank H.-G. Löhmannsröben for access to TCSPC instrumentation, Ming Yau for assistance with peptide synthesis, Bernard Brooks and Richard Pastor for advice on the

Langevin simulations, Milan Hodoscek for implementing the random number generator used in the program CHARMM, Yong Lee and Sergio Hassan for discussion, Jay Knutson for help in lifetime measurements in the initial phases of this work, and Shimon Weiss for a preprint on the length dependence of FRET efficiencies in DNA and sharing other results. Financial support came from the Deutsche Forschungsgemeinschaft and the VolkswagenStiftung.

Figure legends

Fig. 1. (**A**) Molecular model of a polyproline peptide used in this study. The acceptor and donor chromophore are linked to the chain via N- and C-terminal glycine and cysteine residues, respectively. The conformation of the proline 20mer is based on the crystal structure (28), the linkers and dyes were placed in arbitrary orientations. (**B**) Transfer efficiency histograms obtained from confocal single molecule measurements on polyproline peptides of various lengths.

Fig. 2. Mean transfer efficiencies from single molecule measurements (filled red circles) and ensemble time correlated single photon measurements (open red circles) as a function of the contour lengths of the peptides (Gly-Pro$_n$-Cys) assuming the geometry of polyproline found in the crystal structure (28), (**A**) in comparison to the dependences calculated for a rod-like spacer assuming isotropic averaging (solid curve) or a random, but static angular distribution of the dipoles of donor and acceptor (dashed curve) and (**B**) in comparison to the dependences calculated for the different dynamic regimes according to Eq. 4 (dark grey squares), 5 (black squares), and 6 (light grey squares) using the normalized end-to-end distance distributions from the molecular dynamics simulations of the peptides (Fig. 3). The corresponding lines are empirical fits of the data to the equation $E=1/(1+(r/C)^4)$, where C is the fit parameter. The inset to Fig. 2A shows the growing deviation of the transfer efficiency measured in the single molecule experiment (E_m) from the prediction of Eq. 1 (E_F) as the peptide contour length is increased beyond R_0.

Fig. 3. End-to-end distance distributions obtained from molecular dynamics simulations of peptides containing 10, 15, 20, 25, 30, 35 or 40 proline residues plus terminal glycine and cysteine residues (black lines) and the least-squares fits to a wormlike chain model (red lines) using equation 3. Inset: The values for l_c (filled circles) and l_p (open circles) resulting from the fits are shown for the different peptide lengths.

Fig. 4. Timescales of the dynamic processes involved. Indicated are the rotational correlation time of the donor chromophore (blue dashed line), the relaxation time of the autocorrelation function of the end-to-end distance fluctuations calculated from the simulations (green filled circles), and the fluorescence lifetime of the donor dye (red circles) as a function of the number of proline residues in the chain. The typical duration of a photon burst is ~1 ms. The

left inset shows the end-to-end distance autocorrelation function for the polyproline 20mer (green) fit to a single exponential decay (black). The right inset shows the anisotropy decay of the donor chromophore (blue) fit to a double exponential decay (black). The faster component of the decay (0.3 ns) was assigned to the rotational correlation time of the dye (49), and the slower component (0.8 ns) to the rotational correlation time of the entire molecule.

References

1. Stryer, L. & Haugland, R. P. (1967) *Proc. Natl. Acad. Sci. USA* **58,** 719-26.
2. Lakowicz, J. R. (1999) *Principles of Fluorescence Spectroscopy* (Kluwer Academic/Plenum Publishers, New York).
3. Stryer, L. (1978) *Annu. Rev. Biochem.* **47,** 819-846.
4. Haas, E., Katchalskikatzir, E. & Steinberg, I. Z. (1978) *Biopolymers* **17,** 11-31.
5. Selvin, P. R. (2000) *Nature Struct. Biol.* **7,** 730-734.
6. Michalet, X., Kapanidis, A. N., Laurence, T., Pinaud, F., Doose, S., Pflughoefft, M. & Weiss, S. (2003) *Annu. Rev. Biophys. Biomol. Struct.* **32,** 161-182.
7. Ha, T., Enderle, T., Ogletree, D. F., Chemla, D. S., Selvin, P. R. & Weiss, S. (1996) *Proc. Natl. Acad. Sci. USA* **93,** 6264-6268.
8. Jia, Y. W., Talaga, D. S., Lau, W. L., Lu, H. S. M., DeGrado, W. F. & Hochstrasser, R. M. (1999) *Chem. Phys.* **247,** 69-83.
9. Ishii, Y., Yoshida, T., Funatsu, T., Wazawa, T. & Yanagida, T. (1999) *Chem. Phys.* **247,** 163-173.
10. Deniz, A. A., Laurence, T. A., Beligere, G. S., Dahan, M., Martin, A. B., Chemla, D. S., Dawson, P. E., Schultz, P. G. & Weiss, S. (2000) *Proc. Natl. Acad. Sci. USA* **97,** 5179-5184.
11. Talaga, D. S., Lau, W. L., Roder, H., Tang, J. Y., Jia, Y. W., DeGrado, W. F. & Hochstrasser, R. M. (2000) *Proc. Natl. Acad. Sci. USA* **97,** 13021-13026.
12. Ha, T. (2001) *Methods* **25,** 78-86.
13. Schuler, B., Lipman, E. A. & Eaton, W. A. (2002) *Nature* **419,** 743-747.
14. Heyduk, T. (2002) *Curr. Opin. Biotechnol.* **13,** 292-296.
15. Borsch, M., Diez, M., Zimmermann, B., Reuter, R. & Gräber, P. (2002) *Febs Lett.* **527,** 147-152.
16. Lipman, E. A., Schuler, B., Bakajin, O. & Eaton, W. A. (2003) *Science* **301,** 1233-1235.
17. Rhoades, E., Gussakovsky, E. & Haran, G. (2003) *Proc. Natl. Acad. Sci. USA* **100,** 3197-3202.
18. Berney, C. & Danuser, G. (2003) *Biophys. J.* **84,** 3992-4010.
19. Nguyen, V. T., Kamio, Y. & Higuchi, H. (2003) *Embo J.* **22,** 4968-4979.

20. Margittai, M., Widengren, J., Schweinberger, E., Schröder, G. F., Felekyan, S., Haustein, E., König, M., Fasshauer, D., Grubmüller, H., Jahn, R. & Seidel, C. A. M. (2003) *Proc. Natl. Acad. Sci. USA* **100,** 15516-15521.
21. Rasnik, I., Myong, S., Cheng, W., Lohman, T. M. & Ha, T. (2004) *J. Mol. Biol.* **336,** 395-408.
22. Allen, M. W., Urbauer, R. J. B., Zaidi, A., Williams, T. D., Urbauer, J. L. & Johnson, C. K. (2004) *Anal. Biochem.* **325,** 273-284.
23. Klostermeier, D., Sears, P., Wong, C. H., Millar, D. P. & Williamson, J. R. (2004) *Nucleic Acids Res.* **32,** 2707-2715.
24. Slaughter, B. D., Allen, M. W., Unruh, J. R., Urbauer, R. J. B. & Johnson, C. K. (2004) *J. Phys. Chem. B* **108,** 10388-10397.
25. Van Der Meer, B. W., Coker, G. III, Chen, S. Y. S. (1994) *Resonance energy transfer: theory and data* (VCH Publishers, Inc., New York, Weinheim, Cambridge).
26. Förster, T. (1948) *Annalen der Physik* **6,** 55-75.
27. Panchuk-Voloshina, N., Haugland, R. P., Bishop-Stewart, J., Bhalgat, M. K., Millard, P. J., Mao, F. & Leung, W. Y. (1999) *J. Histochem. Cytochem.* **47,** 1179-88.
28. Cowan, P. M. & McGavin, S. (1955) *Nature* **176,** 501-503.
29. Lazaridis, T. & Karplus, M. (1999) *Proteins* **35,** 133-152.
30. Brooks, B. R., Bruccoleri, R. E., Olafson, B. D., States, D. J., Swaminathan, S. & Karplus, M. (1983) *J. Comp. Chem.* **4,** 187-217.
31. Lazaridis, T. & Karplus, M. (1999) *J Mol Biol* **288,** 477-87.
32. Steinbach, P. J. (2004) *Proteins***,** in press.
33. Ryckaert, J.-P., Ciccotti, G. & Berendsen, H. J. C. (1977) *J. Comp. Phys.* **23,** 327-341.
34. Deniz, A. A., Laurence, T. A., Dahan, M., Chemla, D. S., Schultz, P. G. & Weiss, S. (2001) *Annu. Rev. Phys. Chem.* **52,** 233-53.
35. Bhattacharjee, J. K., Thirumalai, D. & Bryngelson, J. D. (1997) *oai:arXiv.org:cond-mat/***,** 9709345.
36. Gopich, I. V. & Szabo, A. (2003) *J. Phys. Chem. B* **107,** 5058-5063.
37. Gopich, I. V. & Szabo, A. (2004) *J. Chem. Phys.* **in press**.
38. Schimmel, P. R. & Flory, P. J. (1967) *Proc. Natl. Acad. Sci. USA* **58,** 52-9.
39. Scholes, G. D. (2003) *Annu. Rev. Phys. Chem.* **54,** 57-87.
40. Wong, K. F., Bagchi, B. & Rossky, P. J. (2004) *J. Phys. Chem.* **108,** 5752-5763.
41. Scholes, G. D. & Fleming, G. R. (in press) *Adv. Chem. Phys.*
42. Henry, E. R. & Hochstrasser, R. M. (1987) *Proc. Natl. Acad. Sci. USA* **84,** 6142-6146.

43. Cantor, C. R., Schimmel, P. R. (1980) *Biophysical Chemistry* (W. H. Freeman & Company.

44. Deniz, A. A., Dahan, M., Grunwell, J. R., Ha, T. J., Faulhaber, A. E., Chemla, D. S., Weiss, S. & Schultz, P. G. (1999) *Proc. Natl. Acad. Sci. USA* **96,** 3670-3675.

45. Kapanidis, A. N., Lee, N. K., Laurence, T. A., Doose, S., Margeat, E. & Weiss, S. (2004) *Proc. Natl. Acad. Sci. USA* **101,** 8936-8941.

46. Hillisch, A., Lorenz, M. & Diekmann, S. (2001) *Curr. Opin. Struct. Biol.* **11,** 201-7.

47. Clegg, R. M., Murchie, A. I., Zechel, A. & Lilley, D. M. (1993) *Proc. Natl. Acad. Sci. USA* **90,** 2994-8.

48. Dale, R. E., Eisinger, J. & Blumberg, W. E. (1979) *Biophys. J.* **26,** 161-193.

49. Alexiev, U., Rimke, I. & Pohlmann, T. (2003) *J. Mol. Biol.* **328,** 705-19.

Figure 1

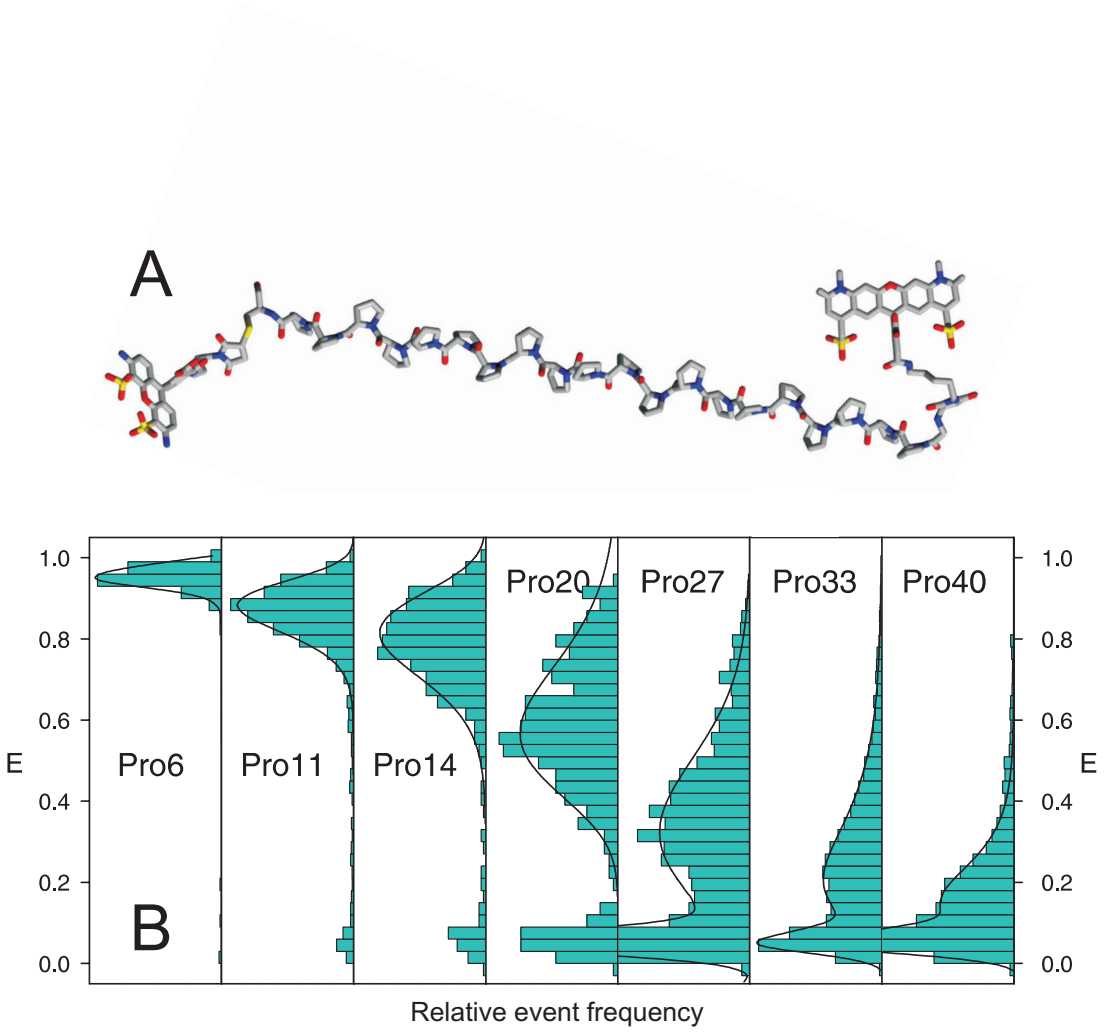
A
B
Pro6
Pro11
Pro14
Pro20
Pro27
Pro33
Pro40
E
E
1.0
0.8
0.6
0.4
0.2
0.0
Relative event frequency

Figure 2

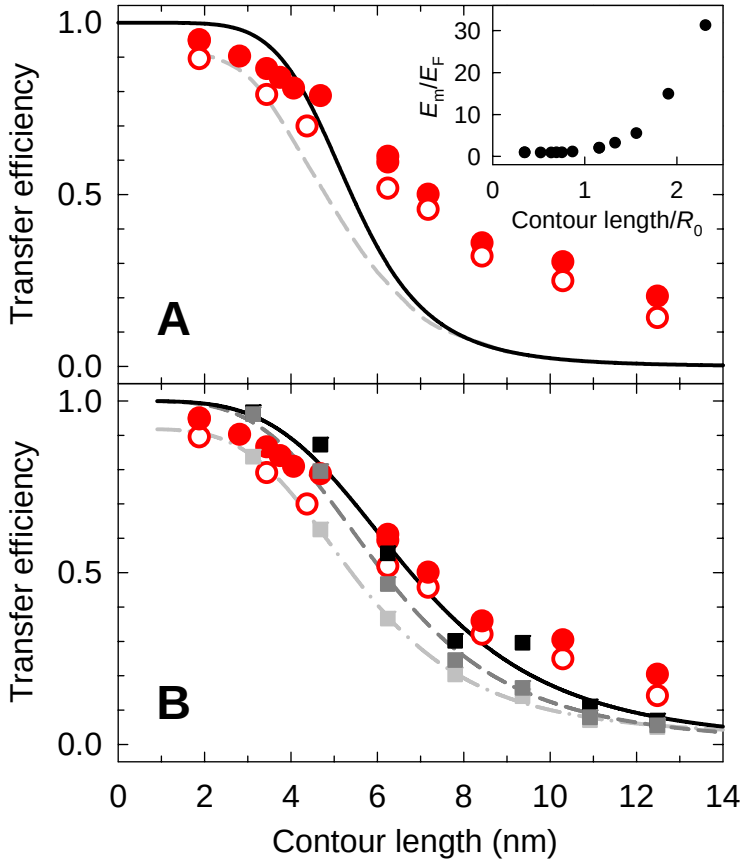
Transfer efficiency
1.0
0.5
0.0
A
B
30
20
10
0
0
1
2
E_m/E_F
Contour length/R_0
0
2
4
6
8
10
12
14
Contour length (nm)

Figure 3

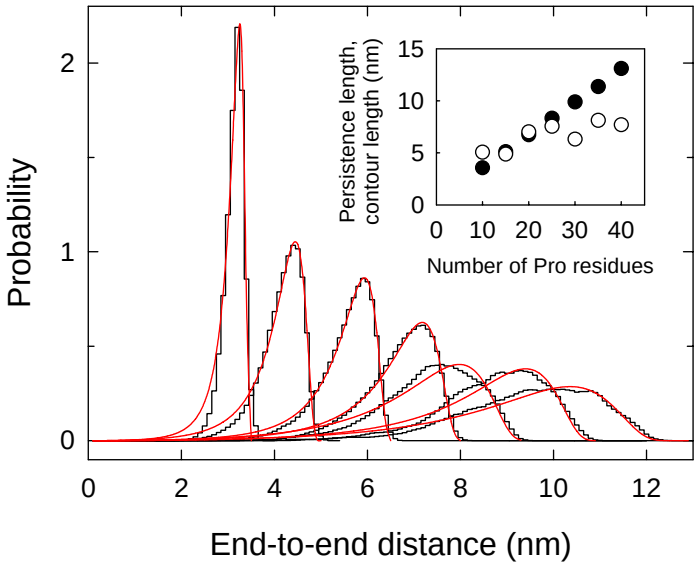
Probability
End-to-end distance (nm)
0
1
2
0
2
4
6
8
10
12
Persistence length, contour length (nm)
Number of Pro residues
0
5
10
15
0
10
20
30
40

Figure 4

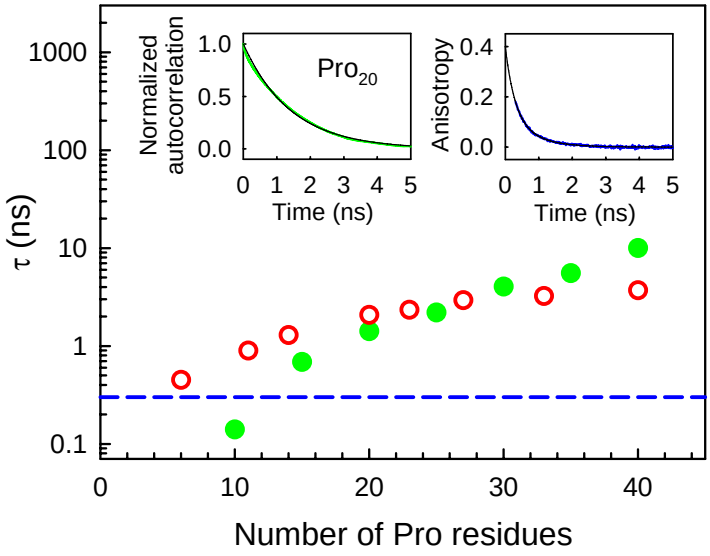
τ (ns)
1000
100
10
1
0.1
0
10
20
30
40
Number of Pro residues
Normalized autocorrelation
1.0
0.5
0.0
Pro20
0 1 2 3 4 5
Time (ns)
Anisotropy
0.4
0.2
0.0
0 1 2 3 4 5
Time (ns)